Sensing and Control of a Multi-Joint Soft Wearable Robot for Upper-Limb Assistance and Rehabilitation

Tommaso Proietti, Ciarán O'Neill, Cameron J. Hohimer, Kristin Nuckols, Megan E. Clarke, Yu Meng Zhou, David J. Lin, and Conor J. Walsh

***Abstract*—In the field of wearable robotics, there has been increased interest in the creation of soft wearable robots to provide assistance and rehabilitation for those with physical impairments. Compared to traditional robots, these devices have the potential to be fully portable and lightweight, a flexibility that may allow for increased utilization time as well as enable use outside of a clinical environment. In this letter, we present a textile-based multi-joint soft wearable robot to assist the upper limb, in particular shoulder elevation and elbow extension. Before developing a portable fluidic supply system, we leverage an off-board actuation system for power and control, with the worn components weighting less than half kilogram. We showed that this robot can be mechanically transparent when powered off, not restricting users from performing movements associated with activities of daily living. Three IMUs were placed on the torso, upper arm and forearm to measure the shoulder and elbow kinematics. We found an average RMSE of ~ 5 degrees when compared to an optical motion capture system. We implemented dynamic Gravity Compensation (GC) and Joint Trajectory Tracking (JTT) controllers that actively modulated actuator pressure in response to IMU readings. The controller performances were evaluated in a study with eight healthy individuals. Using the GC controller, subject shoulder muscle activity decreased with increasing magnitude of assistance and for the JTT controller, we obtained low tracking errors (mean ~ 6 degrees RMSE). Future work will evaluate the potential of the robot to assist with activities in post-stroke rehabilitation.**

***Index Terms*—Rehabilitation robotics, soft robotics, wearable robotics.**

I. Introduction

ASSISTIVE wearable robotics is an emerging trend in the domain of robotics that has been a focus of research groups around the world since the early '90 s. From medical applications (*e.g.*, stroke rehabilitation [1], spinal cord injury assistance [2], etc.) to healthy individuals assistance (*e.g.*, to reduce injuries in workplaces [3], to assist during sport performances [4], etc.), hundreds of assistive wearable robots have been developed in both universities and industry, and we have more recently started observing many of these devices reaching the market and being heavily validated by end-users. Today commercial wearable robots are mostly rigidly framed, with either passively or actively actuated joint, and can provide targeted assistance to one or more human body joints simultaneously [5]. A shortcoming of these rigid robots is their size and weight, requirement for careful alignment between the user joints and the robot ones, relatively high cost and limited portability (particularly if actuated) [6], [7].

A promising new trend in this field is the creation of assistive wearable robots which use soft actuators to directly engage with the human body and to support its movements. In a soft wearable robot, the frame of the robot is the wearer's skeletal structure. The combination of soft actuation methods, like pneumatic textile-based actuators or cable-driven actuators, and the lack of a rigid frame can address many of the aforementioned limits of rigid robots. The inherent compliance of the actuators allows for a more direct, safer and natural physical interaction between the users and the robot. However, the complexity of sensing and controlling this interaction is dramatically increased due to this inherent compliance, which is challenging to model due to the many degrees of freedom involved between the soft actuator and the biological tissues of the user. This challenge can be further complicated when dealing with medical applications and impaired populations whose muscle tone and body composition may vary more broadly than a healthy population.

When considering medical applications such as stroke rehabilitation, the most commonly used wearable robots are rigid *exoskeletons (e.g.*, the ArmIn exoskeleton, commercially available under the name of Armeo Power, Hocoma, Switzerland [17]) and rigid *manipulanda* or end-effector robots (*e.g.*, the MIT-Manus, commercially available under the name of InMotion Arm, Bionik, Canada [18]). Exoskeletons and manipulanda have been evaluated intensively with large populations of stroke survivors and with randomized controlled trials (*e.g.*, [19], [20]). However, the improvements in relevant outcome metrics when comparing robotic assisted therapies with conventional therapies are still limited [8] and therefore the advantage of using these devices is still under discussion [21].

The relative portability of soft robots may allow for seamless integration with the clinical environment, favoring the adoption of robotic-therapy during simulated activities of daily living

Manuscript received October 14, 2020; accepted February 11, 2021. Date of publication February 22, 2021; date of current version March 15, 2021. This letter was recommended for publication by Associate Editor K.-U. Kyung and Editor J.-H. Ryu upon evaluation of the reviewers' comments. This work was supported by the National Science Foundation EFRI under Award 1830896 and Harvard School of Engineering and Applied Sciences. *(Tommaso Proietti and Ciarán O'Neill contributed equally to this work.) (Corresponding author: Conor James Walsh.)*

Tommaso Proietti, Ciarán O'Neill, Cameron J. Hohimer, Kristin Nuckols, Megan E. Clarke, Yu Meng Zhou, and Conor J. Walsh are with the John A. Paulson School of Engineering and Applied Sciences, Harvard University, Cambridge, MA 02139 USA (e-mail: tproietti@g.harvard.edu; ciaranoneill@g.harvard.edu; chohimer@g.harvard.edu; kristin_nuckols@g.harvard.edu; meganclarke@g.harvard.edu; yumengzhou@seas.harvard.edu; walsh@seas.harvard.edu).

David J. Lin is with the Department of Neurology Center for Neurotechnology and Neurorecovery, Massachusetts General Hospital, Harvard Medical School, Boston, MA 02115 USA, and also with the Division of Neurocritical Care and Emergency Neurology, Department of Neurology, Massachusetts General Hospital, Boston, MA 02114 USA (e-mail: dlin7@mgh.harvard.edu).

Digital Object Identifier 10.1109/LRA.2021.3061061

(ADL) scenarios. This portability can also potentially allow the robots to be brought into the homes of those in need of therapy, enabling greater therapy engagement and a greater volume and duration of therapy. In fact, it is important to underline that the limited volume of therapy is still considered the number one cause of limited outcomes of the robot-assisted stroke therapy [22], [23].

The literature of soft wearable assistive and rehabilitation robots is still young and evolving. To the authors' knowledge, very few devices targeting upper-limb assistance (excluding hand) exist and predominantly assist only a single joint. Many of these robots are cable-driven, targeting either the shoulder [12], [13], the elbow [9] or the wrist [14]. Multi joint robots have typically assisted both the shoulder and elbow [15], [16]. Many of these devices have been evaluated on healthy participants but very few have been evaluated on any impaired users. A pneumatic shoulder robot by Simpson *et al.* [10], [11] recently demonstrated reductions in muscle activity and was shown to improve the average range of motion (ROM) across 6 stroke survivors.

In a previous study with 5 stroke survivors, our group demonstrated that a pneumatic shoulder robot can both increase their functional ROM while also reducing the fatigue of a therapist when performing rehabilitation exercises [24]. However, the device was manually controlled to modulate the delivered assistance by a member of the research team. Additionally, based on stroke survivor and therapist feedback during that study, we determined that additional assistance was required at the elbow to fully overcome the *flexor synergy*, whereby stroke survivors often experience involuntary coupling of shoulder abductor activity with activation of elbow flexors.

In this paper, we expanded the existing soft wearable robot for the shoulder to provide assistance with elbow extension, and developed sensing and dynamic control strategies to allow for automatic control of the entire robot. The portability and compliance of the expanded wearable robot may allow for the robot to be used safely outside of clinical settings, where the robot can be donned by untrained caregivers as accurate alignment is not necessary due to the inherent compliance of the robot. This work serves to validate the safety and performance of the newly developed elbow extension hardware, and to test the implemented sensing strategy and controller performance, all with healthy individuals prior to future evaluation of the device performance on stroke survivors.

Fig. 1. The worn element of the multi-joint soft wearable robot is comprised of two main components, a shoulder component and a newly developed elbow component. The robot is powered and controlled by an external fluidic supply, and uses 3 inertial measurement units to measure the current pose of the assisted limb for control feedback purposes.

Fig. 2. The structure and manufacture of the soft wearable elbow component is similar to that of the shoulder component. It combines inextensible textiles with extensible ones to securely anchor the actuators while remaining comfortable. The included straps allow for size adjustment to ensure appropriate fit.

II. Device Design

A. Inflatable Textile-Based Soft Wearable Robot

The shoulder component of the soft wearable robot used in this work is based on the robot described in our previous work [24]. The shoulder component provides gravity compensation to the upper limb using a textile-based pneumatic actuator located in the axilla ([25] for a detailed modeling and characterization of this class of textile-based pneumatic actuators).

The robot now includes a separate elbow component to counteract the effects of the *flexor synergy* by assisting with elbow extension. The elbow component, shown in Fig. 2 consists of a sleeve with a pair of inflatable textile-based actuators. The sleeve is constructed in a similar manner to the shoulder component, of an extensible compression material with select inextensible elements for anchoring. A cutout on the posterior side of the sleeve both locates and provides pressure relief about the olecranon. A zipper is included on the upper half of the sleeve to assist with donning. The actuators are simple cylindrical geometry, sewn on the anterior side of the elbow, offset on either side of the mid-line, to provide assistance with elbow extension. A pair of actuators is used as single larger actuator located along the mid-line tended to twist rather than unfold under loading. Furthermore, the inextensible textile of the sleeve between both actuators act as a sling, evenly distributing the forces of actuation. The anchoring and fit of the actuator can be tuned using the straps located on either side of the olecranon.

B. Controller and Fluidic Supply

An off-board fluidic supply was used for this study to quickly evaluate different actuation and control ideas with large

flexibility, and this off-board solution will help inform the design of a future portable fluidic supplies. The fluidic supply is comprised of ten 3-2 direct operation valves (Humphery, USA) paired together to form 5 channels. Direct operation allows for the valves to operate with no minimum pressure. The input valves are configured as normally-closed and the vent valves as normally-open to ensure that the system is vented in the case of power loss or when the emergency stop is activated. These valves are digitally driven by the controller through a current buffer (Diodes, USA) using a bank of solid-state relays (Sainsmart, USA). System input pressure is controlled by an analog electronic regulator (SMC, Japan). Each channel contains an analog pressure sensor (Honeywell, USA) for pressure feedback. Compressed air is supplied to the regulator from an external air source. The fluidic supply hardware is controlled by a Speedgoat IO183/IO613 machine (Speedgoat, Switzerland) running as a Simulink (Mathworks, USA) real-time target. The controller loop operates at 1 kHz, and interacts with the robot and environment through its various ADC, DAC, DIO, CAN ports.

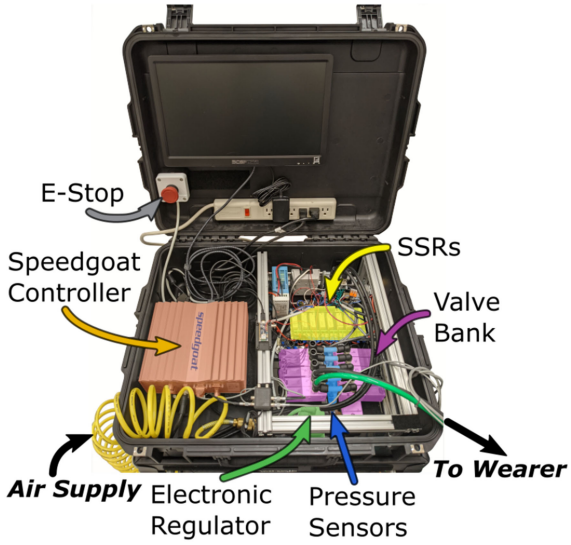

Fig. 3. The off-board fluidic supply and controller was designed to be self contained and fit within a portable case to allow for ease of transport and setup outside of a lab setting.

C. Joint Kinematics Sensing

The robot requires an estimate of the user arm kinematics in order to determine the appropriate assistance to provide through the actuators. This estimation can also be used clinically to quantitatively measure short- and long-term changes in kinematics when the wearer is being assisted by the robot, which may assist the therapists in planning and determining personalized goals of the therapy. Three inertial measurement units (IMUs, Xsens Technologies B.V., the Netherlands) are daisy chained on a CAN-bus and placed on the wearer's torso, upper arm and forearm to measure upper limb pose (shoulder elevation, horizontal flexion, internal-external rotation, and elbow flexion/extension) and torso pose. The IMUs were placed to approximately align their y-axis parallel to the respectively joints rotation axis. The torso IMU acts as the reference orientation which is crucial for arm angle estimation, particularly in medical applications – *e.g.* stroke rehabilitation – to account for trunk compensation which is known to occur during movements of the impaired shoulder.

The angle estimation is performed using rotation matrices provided by the internal Kalman filter of the IMUs. A simple static calibration of the *rest pose* (arm down along the torso) and in *T-pose* (arm abducted at 90 degrees) needs to be performed on startup to zero any angular offsets due to IMU misalignment with the human joints. Drift estimation was not addressed in this work due to the low drift characteristics ($\sim 0.3^{\circ}/min$) specified by the IMU manufacturer and the short duration of each test.

D. Control Strategies

The robot is controlled using a two-layer architecture, as shown in Fig. 4. A low-level control (LLC) loop manages the internal pressure loop via a bang-bang control of the inlet and outlet valves to the pneumatic actuators. The gains of this LLC were manually tuned to achieve the best transient behavior with minimal overshoot. A deadband of ± 3.5 kPa (± 0.5 psi) was experimentally determined to adequately stabilize the LLC output and reduce oscillations. At the same time, a high-level control (HLC) loop uses the data from the IMUs to determine a pressure profile to set the reference for the LLC.

Two different HLCs are implemented: a *Gravity Compensation Control* (GC) and a *Joint Trajectory Tracking Control* (JTT). The objective of the two controllers is to allow for adaptation of the robot assistance to the needs of different users and, in case of medical applications, to the different recovery statuses of the patients, *e.g.* during stroke rehabilitation. The JTT controller is best suited when a wearer has a higher impairment level and requires assistance to initiate and complete any movement. The therapist can easily record the desired trajectory with the robot powered off, thanks to the device's mechanical transparency, and the soft robot can then automatically guide the arm through this trajectory. As the robot guides the arm through the desired motion, the therapist is offloaded so can instead focus on assisting other joints like the wrist or hand, improving the overall effectiveness and quality of the therapy. For wearers who can initiate movements, the GC controller instead allows for more active engagement and more functional therapy.

The GC controller assists the user by dynamically supporting the estimated gravitational load of the limb. This control strategy uses the shoulder and elbow joint angles, as measured by the IMUs, as inputs to a feedforward term which determines the required actuator assistance and commands a pressure profile to the LLC. The feedforward command output can also be scaled to deliver partial gravity compensation. This feedforward term is determined from a calibration routine as illustrated in Fig. 5. The user wears the robot through a pressure sweep from a vented actuator condition to a maximum level of pressure (in this study, ~ 100 kPa for the shoulder actuator and ~ 70 kPa for the elbow actuator), and then back to the vented condition. During the pressure sweeps, the users are asked to relax and their arm is passively mobilized by the robot.

The JTT controller assists the user in following a predefined reference trajectory and can be modulated in order to increase or decrease the assistance as-needed. This strategy uses a PID controller for each controlled joint (shoulder elevation and elbow extension) based on the arm angles as measured by the 3 IMUs on the body of the user. The dynamic response of the JTT

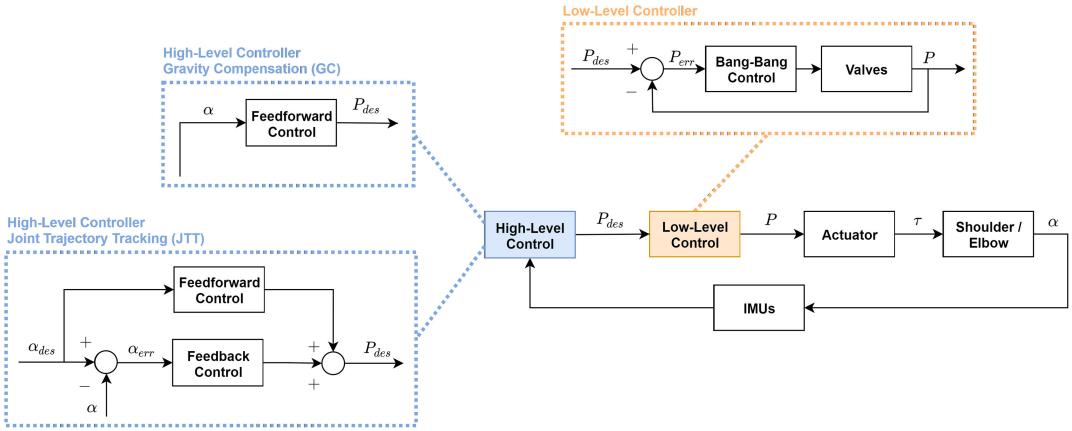

Fig. 4. Low-level control (LLC) and high-level control (HLC) on the soft wearable robot. The LLC is an internal pressure loop to control the valves and regulate the pressure to the pneumatic actuators. The HLC uses the data from the IMUs (user arm angle estimation) to define a pressure profile. α = controlled DOFs (shoulder elevation and elbow extension), τ = torque produced by the actuators, P = pressure.

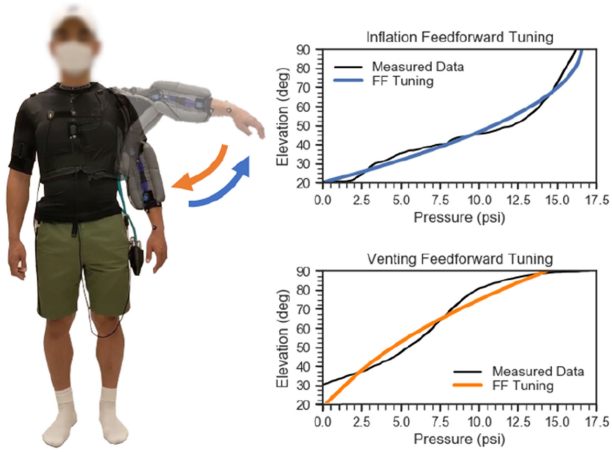

Fig. 5. The tuning of the feedforward term. The user is asked to relax while a pressure sweep is used to map the pressure of the actuator to the resulting angle (two sweeps, one for the shoulder elevation upwards, one for the downward motion).

controller can be improved by including the feedforward element described above for the GC controller, this time fed with the desired trajectory.

III. Methodology

In this study, we focused on validating the performance of our sensing and control strategies on healthy individuals. The study protocol was comprised of three separate tests, performed during a single session. The protocol is shown in Fig. 6. A total of 8 healthy participants (5 male, 3 female, 28.5 ± 3.8 age) volunteered to participate in the study. To fit the different body types (male average weight 81.2 ± 2.7 kg and height 179.8 ± 3.0 cm, female 51.3 ± 1.9 kg and 155.8 ± 3.1 cm), we utilized two sizes of the shoulder device (M for male and XS for female), while the elbow fit all our participants with some adjustments of each individual. A single size of shoulder actuator was used throughout in this study. The study was approved by the Harvard Medical School Institutional Review Board under protocol *IRB19-1321*, and informed consent was obtained from each participant before the protocol was conducted.

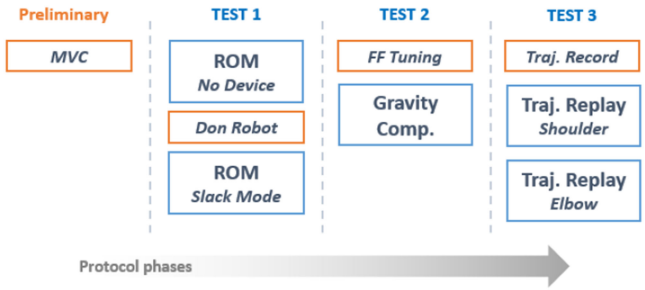

Fig. 6. The three tests of the protocol (in blue) and associated setup (in orange). MVC = Maximum Voluntary Contraction, ROM = Range Of Motion, FF = Feedforward.

A. Preliminary Test: MVC

At the beginning of the study visit, the participants were asked to perform a series of maximum voluntary contractions (MVCs) in order to assess a baseline of maximum muscle activation. This data was used in the post-processing to normalize results across participants. We used 4 surface electromyography (sEMG) sensors (Trigno Avanti, Delsys, USA), sampling data at 2 kHz, to measure activation in the Trapezius Descendens, Biceps Brachii, Triceps Brachii, and Deltoideus Medius. Sensor placement was determined according to SENIAM recommendations for each of the targeted muscles [25].

B. Test 1: Robot Transparency and Sensing Strategy Accuracy

The purpose of the first test was to assess the mechanical transparency of the robot compared to a no-device condition, and the accuracy of the sensing strategy, using a series of single and multi-joint movements as illustrated in Fig. 7. Verifying the mechanical transparency of the robot allows for confidence in the sensing strategy as a transparent robot will enable better coupling of the robots motion to the users motion. The test consisted of 7 specific motions as detailed below, under two conditions, wearing and not wearing the robot. During the robot worn condition, the robot was powered off.

- *Single Joint Motions*
  1) 5x Shoulder Abduction/Adduction ROM, with the elbow full extended.

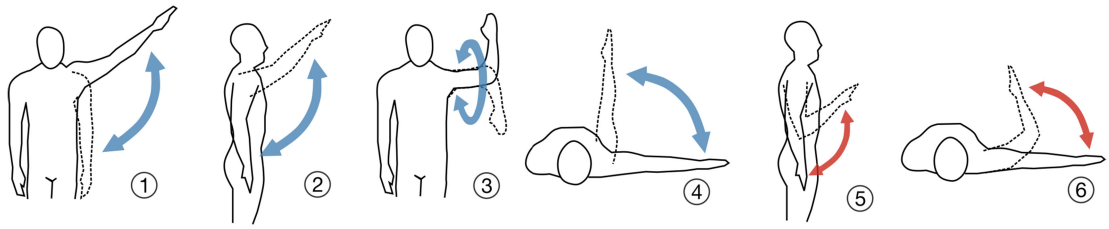

Fig. 7. Illustration of the motion for test 1. In blue, motions involving the shoulder. In red, motions involving the elbow. 1. Shoulder Abduction/Adduction, 2. Shoulder Flexion/Extension, 3. Shoulder Internal/External Rotation, 4. Shoulder Horizontal Flexion/Extension, 5. Elbow Flexion/Extension from rest pose, 6. Elbow Flexion/Extension from T-pose.

2) 5x Shoulder Flexion/Extension ROM, with the elbow full extended.
3) 5x Shoulder Horizontal Flexion/Extension ROM, with the elbow full extended.
4) 5x Shoulder Internal/External Rotation ROM from the T-pose, with the elbow flexed at 90°.
5) 5x Elbow Flexion/Extension ROM from the rest pose.
6) 5x Elbow Flexion/Extension ROM from the T-pose.

- *Multi-Joint Motions*
  1) 10x Random Reaching Motions in the workspace of the user.

C. Test 2: Gravity Compensation Control

The second test was designed to validate the performance of the GC controller. Before beginning controller evaluation, the feedforward term was determined by following the procedure explained in Section II-D. Participants were asked to cyclically abduct their arm from a rest pose to an elevation of about 90° over the course of 4 s, hold that pose for 4 s and then adduct their arm back to the rest pose over 4 s. The movement speed was controlled using a metronome. The motion duration emulates the typical speed of therapy exercises with the aim of reducing the likelihood of triggering spasticity, which can occur during quick movements.

This cycle was repeated three times for each condition. Assistance is defined as the percentage of the calibrated FF output used to assist the joint, with 100% assistance corresponding to complete gravity compensation of the joint. During the first condition, the participants received no assistance for the first set of movements, during the second condition 50% assistance was delivered, and finally 100% gravity compensation was delivered during the third condition. The elbow actuator was inflated throughout this test to maintain a consistent elbow angle between conditions. During this test, the four sEMG sensors recorded the muscle activity in order to verify that the muscles were being offloaded by the robot.

D. Test 3: Joint Trajectory Tracking Control

To begin the final test, two different single-joint trajectories were recorded respectively for the shoulder and the elbow. For the shoulder, two elevations $0° \rightarrow 90° \rightarrow 0°$, followed by a three-step elevation $0° \rightarrow 45° \rightarrow 90° \rightarrow 45° \rightarrow 0°$ were performed. A similar profile was requested for the elbow, with the angle moving from about 90° to 180° in this case. The shoulder trajectory was recorded with the participant standing still, while for the elbow, the participants laid supine on a stretcher with their upper arm pointed up in the air to allow for elbow extension against gravity.

During the controller evaluation, participants were asked to remain relaxed within the robot, while the robot control actuated the target joints to reproduce the previously recorded trajectories. The trajectories were replayed with the feedback-only controller, and a combined feedback/feedforward controller using the calibrated feedforward element of the GC controller. During this test, the four sEMG sensors recorded the muscle activity in order to verify that the wearer did not use their muscles. IMU data was used to measure the wearer movement and drive the controller to track the desired joint trajectory, as discussed in Section II-D.

E. Metrics and Data Processing

An optical motion capture system (Qualisys, Sweden), using 13 reflective passive markers along the upper-body, measured participant's range of motion at 100 Hz. This optical motion capture was used as the ground truth to assess the accuracy of our sensing strategy. Motion caption markers were placed in the same configuration as our previous work [24]. Data was processed in Qualisys Track Manager (Qualisys, Sweden), with joint angles and rotations calculated according to the ISB recommendations for joint orientations and rotation order [26].

In the first test, we assessed sensing strategy accuracy and additionally hardware transparency. For sensing strategy accuracy, the root mean squared error (RMSE) between the joint angles estimated by the IMUs and the optical motion capture was computed. To evaluate hardware transparency, we compared sEMG activation (muscle activity modifications due to the presence of the robot) and motion capture data (potential ROM reduction) between the powered off and no-robot conditions.

To assess the performance of the GC controller, we measured and compared the muscle activation from the four sEMG sensors between the different conditions (no assistance vs 50% of assistance vs 100%). The sEMG data was sampled at 2 kHz and then processed by following the same procedure of our previous work [24]: first band-pass filtered (4th order, 10-400 Hz), then rectified before passing through a final low pass filter (4th order, 10 Hz). Changes in muscle activation due to assistance from the GC controller acts as a proxy metric to verify that the system does unload the shoulder joint. To validate the JTT controller, the RMSE between the desired and the replayed trajectory was computed. Joint angles were collected by using IMUs data only.

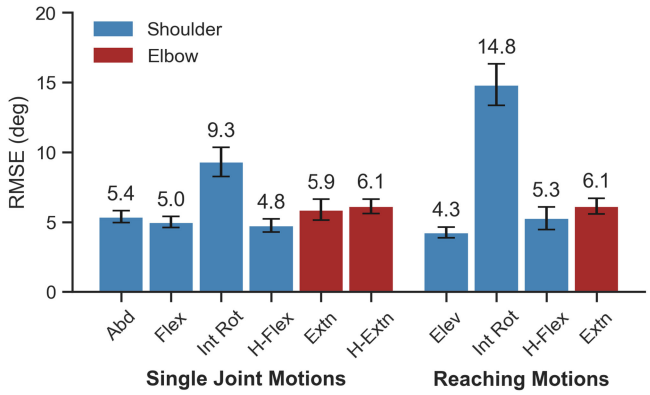

Fig. 8. IMU-based upper-limb joint measurement validation: mean RMSE and standard error across all participants (8) between the IMUs estimated joint angles and the ground truth joint angles from the optical motion capture system.

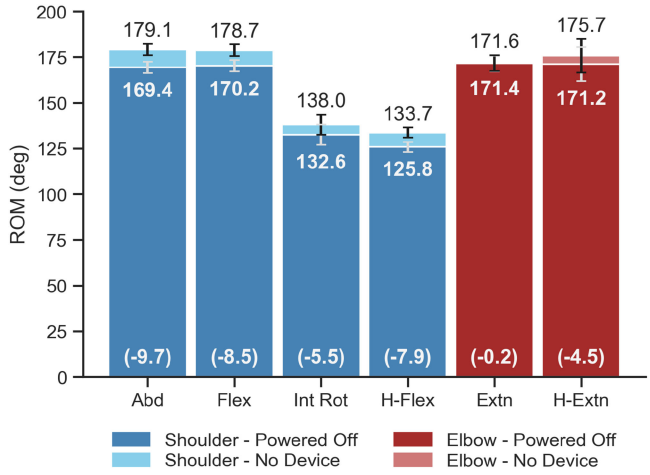

Fig. 9. Robot mechanical transparency test: mean range of motion and standard error of the user without and with the robot powered off, over the eight participants, as measured by the optical motion capture. The number between parenthesis is the reduced ROM.

IV. Results & Discussion

A. Joint Kinematics Measurement

The comparison of the participants measured joint angles, as measured by the optical motion capture and the worn IMUs, is depicted in Fig. 8. The RMSE averaged ~ 5 degrees for most joints over the entire movement during the single joint motions and multi-joint reaching, except for internal/external rotation. The large RMSE for the internal/external rotation axis is likely due to poor coupling of the axial rotation of the humerus through the soft tissue of the upper arm to the IMU on the surface. A future investigation on how to improve this estimation is needed in order to use the soft wearable robot as an assessment tool during stroke rehabilitation. The low RMSE during reaching motions, which involves the synchronous motion of multiple joints, is promising as these reaching motions better emulate motions that occur while performing daily activities in contrast to isolated, single joint motions. IMU drift was not observed, however, the duration of each of our tests was less than five minutes and a new IMU calibration was performed at the beginning of each test.

B. Robot Mechanical Transparency

The mechanical transparency of the wearable robot is highlighted in Fig. 9. When worn and powered off, no tangible increase in muscle activity ($<1\%$) was observed during user initiated motions. However, a slight reduction in total ROM was measured at the limits of motion. These reductions, as measured by the optical motion capture system, were within ~ 10 degrees of when the participants were not wearing the suit, for all the tested DOFs. This minor reduction in maximum ROM was expected as the extensible textile elements have a non-linear stiffness which can become pronounced under large deformation, as occurs near the limits of motion. The minor reduction on ROM should not affect individuals with clinical impairments as the joint ROMs required to complete ADLs is significantly smaller than the biological maximum ROM.

The lack of restriction of the participants clearly demonstrates a key design benefit of soft wearable robot over rigid framed wearable robots, and it is important to maintain this mechanical transparency when working with clinical populations who already suffer from reduced ROM and muscle strength, in particular allowing a therapist to freely manipulate the limb when the device is powered off. Moreover, the transparency of the robot also ensures good coupling of the robot to the wearer which assists in maintaining the desired alignment of the sensors and actuators over the majority of the wearers ROM.

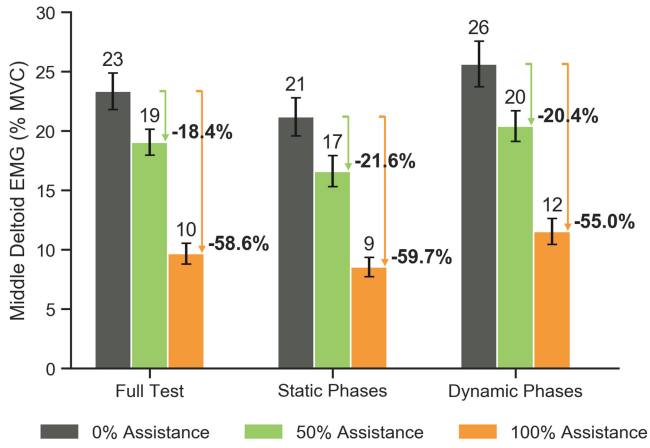

Fig. 10. Gravity Compensation Control validation: mean sEMG changes and standard error in the Middle Deltoid over the full test and the static and dynamic phases only, between the unassisted and assisted conditions. Values are percentages with respect to the participant's MVC. In bold, reduction of muscle activity when assisted compared to the 0% assistance case.

C. Gravity Compensation Control

The muscle activity of the Middle Deltoid (MD), the primary muscle for shoulder abduction, in response to the GC controller is depicted in Fig. 10. As expected, the general trend in muscle activity demonstrates that with increased assistance, there were proportionally greater reductions in the MD activity. Minor reductions were also observed in the other measured muscles, as shown in Table I. It is also clear that the GC controller allowed for meaningful assistance to be provided not just while static but also while the arm was in motion, as shown in Fig. 10.

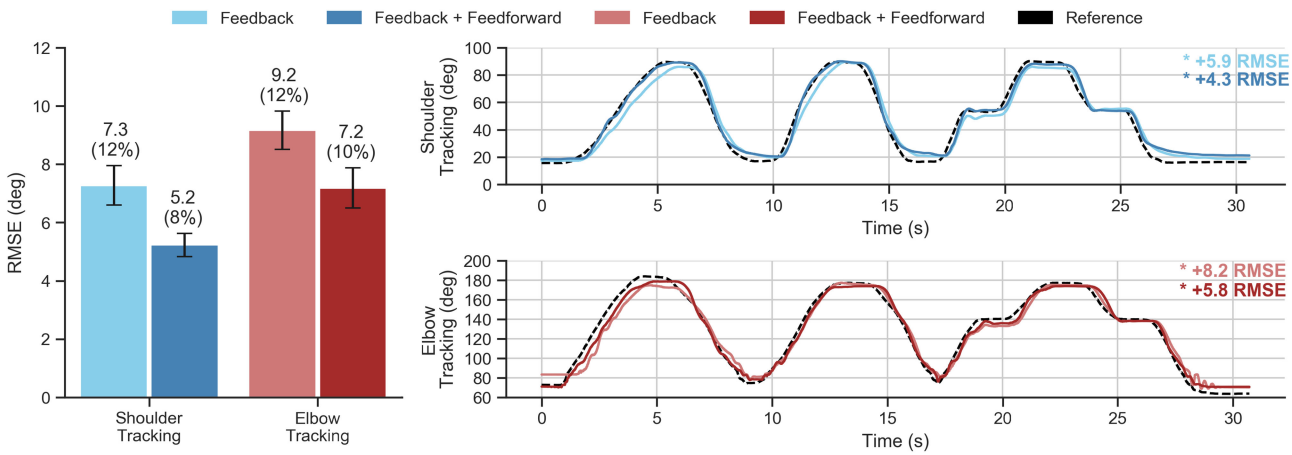

Fig. 11. Joint Trajectory Tracking Control validation. On the left, mean RMSE and standard error of the replayed trajectory with respect to the reference joint trajectory of the 8 participants, as measured by the IMUs. In parenthesis, the percentage of RMSE error compared to the range of the motion. On the right, an example of one participants trajectories, with resulting RMSEs.

TABLE I
MEAN SEMG AND STANDARD ERROR IN OTHER MONITORED MUSCLES. VALUES ARE PERCENTAGES WITH RESPECT TO PARTICIPANT'S MVC

	Trapezious	Biceps	Triceps
0% Assistance	20.0 ± 1.6	4.65 ± 0.5	3.9 ± 0.2
50% Assistance	17.4 ± 1.0	3.31 ± 0.4	3.3 ± 0.1
100% Assistance	17.0 ± 1.3	2.32 ± 0.3	3.4 ± 0.1

D. Joint Trajectory Tracking Control

The tracking error of the JTT controller is aggregated in Fig. 11, in addition to two examples of joint trajectory plots measured using the IMUs. The measured RMSE is small for both the tested conditions: the feedback only condition and the feedback plus feedforward condition, with the latter experiencing an expected reduction in RMSE due to the improved dynamic response of the control (better tracking of the transitory phases). The observed improvements due to the feedforward controller make conducting the simple feedforward calibration worthwhile even if the GC controller is not being used.

The shoulder tracking achieved better results than the elbow. This may be due to the accuracy of our low-level pressure controller, which had a set deadband of ± 3.5 kPa (± 0.5 psi) for both joints. The relative torque, and thus pressure required at the elbow was significantly lower than the required torque/pressure of the shoulder actuator, with the elbow actuator operating at approximately half the pressure of the shoulder, thus doubling the relative hysteresis and reducing controller accuracy.

Despite the promising tracking accuracy, we found that the JTT controller was adversely affected by the limited ability of the actuators to vent at low angles (as can be seen in Fig. 11). When the average RMSE for the 8 participants was recalculated excluding elevation angles below 30 degrees, the RMSE for these higher shoulder elevation angles was reduced to 4.9° and 2.2° respectively for feedback control only and combined feedback + feedforward control. A similar effect was observed at the elbow, limiting the analysis range to elbow extension angles $> 80^\circ$, with a RMSE of 4.7° and 3.4° again for feedback only and the combined feedback + feedforward control. It is important to underline how these RMSE values represent a worst case scenario, in which the participants make no attempt to assist in completing the trajectory (as confirmed by the sEMG data which remained below 4% of activation for all the muscles, at all times in all condition), requiring the robot and controller to fully replicate the desired trajectory.

V. CONCLUSION

In this study, we designed and validated the sensing and control strategies for a multi-joint soft wearable robot intended to provide assistance and rehabilitation to the upper-limb. We demonstrated that the robot was capable of automatically controlling the shoulder elevation and elbow extension of the wearer, actively inflating or venting the pneumatic textile-based actuators in response to the users motions. By comparing users natural motion to that when they were wearing the system but with it powered off, we highlighted the device's inherent mechanical transparency which allows the wearers to achieve most of their natural workspace (less than 10° of reduction at the extreme of the joint ROM), without a tangible increase in their muscle activity. This transparency also enables better coupling of the robots motion to the users motion, which may enable the device to be used as an assessment tool when in its powered off state. The accuracy of the employed IMU-based sensing strategy was also evaluated through comparison with measurements from an optical motion capture system. Results showed small RMSEs (below 6° for all the measured DOFs but the internal/external rotation which resulted in slightly higher RMSE), which may allow this IMU-based sensing strategy to be used to estimate meaningful kinematic metrics without the need to use an external optical motion capture system. IMU drift was not observed in the sensor based measurements, likely in part due to the short time period required for each test (less than 5 minutes per test) and a calibration being performed at the beginning of every test. Future studies will target improving the current calibration methodology (which is fast but still requires 2 static poses), by investigating online automatic re-calibration strategies to compensate for any drift of the IMUs.

Despite the mechanical transparency of the robot, it was still capable of providing meaningful assistive torques to the participants. The robot was able to reduce the effect of gravity at the shoulder by using a feedforward controller, and provide full joint support while replaying prerecorded joint trajectories with a minimal residual error ($\sim 5^\circ$ RMSE at the shoulder and $\sim 7^\circ$ RMSE at the elbow). The results of tracking are particularly promising, enabling patients with limited or no active motor function to complete movement therapy while assisted by the robot. Future work will focus on improving low-level pressure control at low angles, where most of the RMSE was accumulated. The simple nature of the feedforward control allowed for control of the robot despite the low internal/external rotation estimation accuracy. The off-board fluidic supply used in this study serves as a development and assessment platform to determine the specification for future, portable fluidic supplies which will enable use of the robot in unstructured environments, such as a patient's house. A limitation for this study was the validation on healthy participants only. Now that the controllers have been validated on-body, future studies will aim to assess the effects of the controllers with stroke survivors in a context of physical rehabilitation and in the potential presence of unnatural patterns of movements (like the flexor synergy) and/or compensation strategies typical of this population. Additionally, we plan to investigate longitudinal utilization of the multi-joint robot during rehabilitation therapy in order to assist both the user and the caregiver. Specifically, we see potential for improving the engagement and active participation of the stroke survivors in the hope of better clinical outcomes, and as an assessment tool to better quantify patient improvement over time.

REFERENCES

[1] T. Proietti, V. Crocher, A. Roby-Brami, and N. Jarrassé, "Upper-limb robotic exoskeletons for neurorehabilitation: A review on control strategies," *IEEE Rev. Biomed. Eng.*, vol. 9, pp. 4–14, Apr. 2016, doi: 10.1109/RBME.2016.2552201.

[2] M. Mekki *et al.*, "Robotic rehabilitation and spinal cord injury: A narrative review," *Neurotherapeutics*, vol. 15, pp. 604–617, 2018.

[3] T. Butler and J. Gillette, "Exoskeletons: Used as PPE for injury prevention," *Kinesiol. Pub.*, vol. 47, pp. 33–37, 2019.

[4] *ROAM Robotics*, 2021. [Online]. Available: roamrobotics.com/ski

[5] P. Maciejasz *et al.*, "A survey on robotic devices for upper limb rehabilitation," *J. Neuroeng. Rehabil.*, vol. 11, no. 1, pp. 1–29, 2014.

[6] M. A. Gull *et al.*, "A review on design of upper limb exoskeletons," *Robotics*, vol. 9, no. 1, p. 16, 2020, doi: org/10.3390/robotics9010016.

[7] R. Gopura *et al.*, "Developments in hardware systems of active upper-limb exoskeleton robots: A review," *Robot. Auton. Syst.*, vol. 75, Part B., pp. 203–220, 2016.

[8] J. Mehrholz *et al.*, "Systematic review with network meta-analysis of randomized controlled trials of robotic-assisted arm training for improving activities of daily living and upper limb function after stroke," *J. Neuro-Engineering Rehabil*, vol. 17, no. 1, pp. 1–14, 2020.

[9] M. Xiloyannis *et al.*, "Physiological and kinematic effects of a soft exosuit on arm movements," *J. NeuroEngineering Rehabil*, vol. 16, no. 1, pp. 1–15, 2019.

[10] C. Simpson *et al.*, "Exomuscle: An inflatable device for shoulder abduction support," in *Proc. IEEE Int. Conf. Robot. Automat.*, 2017, pp. 6651–6657.

[11] C. Simpson, B. Huerta, S. Sketch, M. Lansberg, E. Hawkes and A. Okamura, "Upper extremity exomuscle for shoulder abduction support," *IEEE Trans. Med. Robot. Bionics*, vol. 2, no. 3, pp. 474–484, Aug. 2020.

[12] D. Park and K. J. Cho, "Development and evaluation of a soft wearable weight support device for reducing muscle fatigue on shoulder," *PLoS ONE*, vol. 12, no. 3, 2017, Art. no. e0173730.

[13] S. B. Kesner *et al.*, "Design considerations for an active soft orthotic system for shoulder rehabilitation," in *Proc. Annu. Int. Conf. IEEE Eng. Med. Biol. Soc.*, 2011, 8130–8134.

[14] H. Choi, B. B. Kang, B. Jung, and K. Cho, "Exo-wrist: A soft tendon-driven wrist-wearable robot with active anchor for dart-throwing motion in hemiplegic patients," *IEEE Robot. Automat. Lett.*, vol. 4, no. 4, pp. 4499–4506, Oct. 2019.

[15] I. Gaponov *et al.*, "Auxilio: A portable cable-driven exosuit for upper extremity assistance," *Int. J. Control Autom. Syst.*, vol. 15, no. 1, pp. 73–84, 2017.

[16] S. Lessard, P. Pansodtee, A. Robbins, J. M. Trombadore, S. Kurniawan, and M. Teodorescu, "A soft exosuit for flexible upper-extremity rehabilitation," *IEEE Trans. Neural Syst. Rehabil. Eng.*, vol. 26, no. 8, pp. 1604–1617, Aug. 2018.

[17] A. Power, Hocoma, 2021. [Online]. Available: hocoma.com/us/solutions/armeo-power

[18] *InMotion Arm, Bionik*, 2021. [Online]. Available: bioniklabs.com/products/inmotion-Arm

[19] H. Rodgers *et al.*, "Robot assisted training for the upper limb after stroke (RATULS): A multicentre randomised controlled trial," *Lancet*, vol. 394, no. 10192, pp. 51–62, 2019.

[20] V. Klamroth-Marganska *et al.*, "Three-dimensional, task-specific robot therapy of the arm after stroke: A multicentre, parallel-group randomised trial," *Lancet Neurol.*, vol. 13, no. 2 pp. 159–166, 2014.

[21] C. Duret *et al.*, "Robot-assisted therapy in upper extremity hemiparesis: Overview of an evidence-based approach," *Front. Neurol.*, vol. 10, no. 412, 2019, doi: 10.3389/fneur.2019.00412.

[22] M. S. Jeffers *et al.*, "Does Stroke Rehabilitation Really Matter? Part B: An Algorithm for Prescribing an Effective Intensity of Rehabilitation," *Neurorehabilitation Neural Repair.*, vol. 32, no. 1, pp. 73–83, 2018.

[23] V. Huang and J. Krakauer, "Robotic neurorehabilitation: A computational motor learning perspective," *J. Neuroeng. Rehabil.*, vol. 6, no. 1, pp. 1–13, 2009.

[24] C. O'Neill *et al.*, "Inflatable soft wearable robot for reducing therapist fatigue during upper extremity rehabilitation in severe stroke," *IEEE Robot. Automat. Lett.*, vol. 5, no. 3, pp. 3899–3906, Jul. 2020.

[25] *Recommendations for Sensor Locations on Individual Muscles*, 2021. [Online]. Available: http://seniam.org/sensor_location.htm

[26] G. Wu *et al.*, "ISB recommendation on definitions of joint coordinate systems of various joints for the reporting of human joint motion - part II: Shoulder, elbow, wrist and hand," *J. Biomech.*, vol. 38, no. 5, pp. 981–992, 2005.